AGU PUBLICATIONS

Geophysical Research Letters

RESEARCH LETTER
10.1002/2017GL073758

**Key Points:**
- The upwelling rate of anthropogenic carbon from the thermocline to the surface layer is almost twice as large as air-sea fluxes
- Diffusion has a major impact on reemergence of anthropogenic carbon in the Equatorial Pacific
- Reemergence of anthropogenic carbon decreases dramatically during the El Niño events

**Supporting Information:**
- Supporting Information S1

**Correspondence to:**
P. Zhai,
pzhai@princeton.edu

**Citation:**
Zhai, P., Rodgers, K. B., Griffies, S. M., Slater, R. D., Iudicone, D., Sarmiento, J. L., & Resplandy, L. (2017). Mechanistic drivers of reemergence of anthropogenic carbon in the equatorial pacific. *Geophysical Research Letters*, *44*. https://doi.org/10.1002/2017GL073758

Received 6 APR 2017
Accepted 7 SEP 2017
Accepted article online 12 SEP 2017



# Mechanistic Drivers of Reemergence of Anthropogenic Carbon in the Equatorial Pacific

**Ping Zhai[1], Keith B. Rodgers[1], Stephen M. Griffies[2], Richard D. Slater[1], Daniele Iudicone[3], Jorge L. Sarmiento[1], and Laure Resplandy[4]**

[1]AOS Program, Princeton University, Princeton, NJ, USA, [2]NOAA/GFDL, Princeton, NJ, USA, [3]Stazione Zoologica Anton Dohrn, Naples, Italy, [4]Geosciences and PEI, Princeton University, Princeton, NJ, USA

**Abstract** Relatively rapid reemergence of anthropogenic carbon ($C_{ant}$) in the Equatorial Pacific is of potential importance for its impact on the carbonate buffering capacity of surface seawater and thereby impeding the ocean's ability to further absorb $C_{ant}$ from the atmosphere. We explore the mechanisms sustaining $C_{ant}$ reemergence (upwelling) from the thermocline to surface layers by applying water mass transformation diagnostics to a global ocean/sea ice/biogeochemistry model. We find that the upwelling rate of $C_{ant}$ (0.4 PgC $yr^{-1}$) from the thermocline to the surface layer is almost twice as large as air-sea $C_{ant}$ fluxes (0.203 PgC $yr^{-1}$). The upwelling of $C_{ant}$ from the thermocline to the surface layer can be understood as a two-step process: The first being due to diapycnal diffusive transformation fluxes and the second due to surface buoyancy fluxes. We also find that this reemergence of $C_{ant}$ decreases dramatically during the 1982/1983 and 1997/1998 El Niño events.

## 1. Introduction

To date, subpolar and high-latitude regions have been the main focus of studies of ocean carbon-climate feedbacks, over both the North Atlantic (Halloran et al., 2015; Schwinger et al., 2014) and the Southern Ocean (Hauck & Völker, 2015; Le Quéré et al., 2007; Sarmiento et al., 1998). It was originally expected that waters comprising deep, intermediate, and subpolar water masses should dominate anthropogenic carbon ($C_{ant}$) accumulation (Sabine et al., 2004). However, more recent consideration of $C_{ant}$ accumulation revealed that 34% of the WOCE (the World Ocean Circulation Experiment) era inventories resided in waters shallower than the base of the directly ventilated thermocline (potential density $\sigma < 26.6$ kg $m^{-3}$) (Iudicone et al., 2016). One of the most important overturning structures within the thermocline are the subtropical cells (STCs), which link subtropical subduction regions with equatorial upwelling regions. These STC structures could support rapid (decadal) reemergence of $C_{ant}$ from the ocean interior back into the surface layers, in particular, in the Equatorial Pacific (Bopp et al., 2015; Iudicone et al., 2016; Nakano et al., 2015), with potentially important implications for carbon-climate feedbacks. The potential for strong re-emergence on decadal time scales is already in evidence with the evolution of the bomb-radiocarbon transient in the Equatorial Pacific (Guilderson & Schrag, 1998; Rodgers et al., 2004). For the case considered here, high dissolved inorganic carbon (DIC) waters resulting from $C_{ant}$ reemergence in obduction or upwelling regions would perturb the Revelle factor of local surface waters and thereby inhibit local uptake of $C_{ant}$ via gas exchange.

Lévy et al. (2013) and Bopp et al. (2015) demonstrated the importance of net upwelling of DIC into the mixed layer in the Equatorial Pacific and identified as well a nontrivial role for diffusion of DIC across the base of the mixed layer, by applying instantaneous kinematic subduction and obduction diagnostics to a global model of the carbon cycle. However, they did not identify a specific connection to the shallow overturning circulation structures in which the Equatorial Pacific carbon cycle is embedded.

Our objective is to build upon these previous efforts to identify the mechanisms that sustain the reemergence of $C_{ant}$ in the Equatorial Pacific. We examine the processes controlling the upwelling, or reemergence, of $C_{ant}$ using a water mass transformation framework that isolates the contributions from surface buoyancy forcing, tracer diffusion, and other processes. In this context, upwelling is defined as the net upward diapycnal transport of $C_{ant}$, which can have both vertical and horizontal components depending on the local isopycnal slopes. A principal advantage of applying the water mass transformation diagnostics is to provide an intrinsic connection between the diapycnal transport of $C_{ant}$ and the overturning circulation that is not provided by kinematic subduction/obduction diagnostics. Iudicone et al. (2011) illustrated the utility of this

approach for studying the natural carbon cycle in the Southern Ocean, whereas we focus on overturning circulation of $C_{ant}$ in the Equatorial Pacific. In this study, our focus is on understanding the mechanisms that control the transport of $C_{ant}$ from the thermocline to the surface layer in the Equatorial Pacific by applying the water mass transformation framework to a global ocean/sea ice/biogeochemistry model.

## 2. Model Description

We use the Geophysical Fluid Dynamics Laboratory's (GFDL's) Modular Ocean Model 5 (MOM5) (Griffies, 2012), configured according to the ocean/sea ice components of GFDL's Earth System Model ESM2M (Dunne et al., 2012, 2013). The ocean configuration has 50 vertical levels with a nominal 1° horizontal resolution, refined meridionally to 1/3° near the equator to capture key features of the equatorial current system. The vertical mixing parameterization most relevant for the equatorial thermocline region includes the shear-mixing component of the K-Profile Parameterization (KPP) boundary layer scheme of Large et al. (1994), as well as a constant background diffusivity of $10^{-5}$ $m^2$ $s^{-1}$. The ocean biogeochemistry model is Tracers of Phytoplankton with Allometric Zooplankton (TOPAZ) code version 2.0 documented in Dunne et al. (2013).

The ocean/sea ice model was spun up for more than 1,000 years with normal year (climatological) forcing derived from the Coordinated Ocean-ice Reference Experiments (CORE) version 2 product (Large & Yeager, 2009), with TOPAZ run online with preindustrial atmospheric $CO_2$ boundary conditions. Subsequently, the model run was split into two separate simulations with normal year forcing, one that maintains constant preindustrial atmospheric $CO_2$ and one that includes the transient atmospheric $CO_2$ during the period of 1860–1947. The circulation for both of these experiments is identical, and the difference in the carbon state variables defines the anthropogenic transient signal. The two model runs were then forced by one cycle of the interannually varying CORE 2 surface forcing (Large & Yeager, 2009) spanning 1948–2007. The model output used in this study is 5 day means spanning the period of 1980–2000. $C_{ant}$ in our model simulation compares well with observational-based data product. A more detailed comparison can be found in the supporting information (Key et al., 2004; Khatiwala et al., 2009; Le Traon et al., 2003; Pascual et al., 2006; Trenberth, 1997).

## 3. Method

In this study, we examine the $C_{ant}$ budget in the Equatorial Pacific between 15°S and 15°N. In this region, the evolving $C_{ant}$ distribution depends on the overturning circulation and the associated meridional transport across 15°S and 15°N, the diapycnal transport, the air-sea fluxes, all diagnosed from the 5 day mean model output fields.

We further decompose the diapycnal transports of $C_{ant}$ ($T(\sigma)$) into the diapycnal diffusive transport of $C_{ant}$ (Cd) and the diapycnal transport due to water mass transformation ($\Phi$), using the water mass transformation framework of Iudicone et al. (2011), which was previously applied to study the Southern Ocean carbon cycle. As we are focused on upper ocean equatorial waters, we consider the water mass transformation diagnostics based on potential density referenced to surface pressure. In the framework developed by Iudicone et al. (2011), the net diapycnal transport ($T(\sigma)$) of an arbitrary tracer $c$ across an isopycnal surface $S_\sigma$ is calculated by

$$\begin{aligned} T(\sigma) &= \mathrm{Cd}(\sigma) + \Phi(\sigma) \\ \mathrm{Cd}(\sigma) &= \int_{S_\sigma} \boldsymbol{J}^{C_{ant}} \cdot \mathrm{d}\boldsymbol{S} \\ \Phi(\sigma) &= \frac{\partial}{\partial \sigma} \int_{V(\sigma_0,\sigma)} c \frac{\mathrm{d}\sigma}{\mathrm{d}t} \mathrm{d}V \end{aligned} \tag{1}$$

where $\mathrm{Cd}(\sigma)$ is a diapycnal diffusive transport of tracer crossing the isopycnal surface $S_\sigma$, with this transport associated with the spatial gradient of $C_{ant}$ used to compute the subgrid-scale flux $\boldsymbol{J}^{C_{ant}}$. $\Phi(\sigma)$ is a diapycnal transport arising from water mass transformation which is associated with motions relative to isopycnals. The density $\sigma_0$ is an arbitrary reference density surface, and $V(\sigma_0, \sigma)$ is a volume bounded by the isopycnal surfaces $S_\sigma$ and $S_{\sigma_0}$. The diapycnal transports $\Phi(\sigma)$ and $\mathrm{Cd}(\sigma)$ are defined as positive when transports are toward denser water. For a discrete diagnostic calculation, $\Phi(\sigma)$ is estimated by

$$\Phi(\sigma) = \frac{\partial}{\partial \sigma} \int_{V(\sigma_0,\sigma)} c \frac{\mathrm{d}\sigma}{\mathrm{d}t} \mathrm{d}V \approx \frac{1}{\delta\sigma} \int \mathrm{d}x\, \mathrm{d}y \int_{z(\sigma-\delta\sigma/2)}^{z(\sigma+\delta\sigma/2)} c \frac{\mathrm{d}\sigma}{\mathrm{d}t} \mathrm{d}z. \tag{2}$$

where $\delta\sigma$ is a discrete potential density interval, and d$x$, d$y$, and d$z$ are model grid cell sizes. In the evaluation of $\Phi(\sigma)$, we chose a potential density binning interval of $\delta\sigma$ = 0.1 kg m$^{-3}$. In equation (2), the material time evolution of the potential density equation can be written as

$$\frac{\mathrm{d}\sigma}{\mathrm{d}t} = \frac{1}{\rho_0}\frac{\partial\sigma}{\partial\Theta}\left(\frac{\mathrm{d}\Theta}{\mathrm{d}t}\right) + \frac{1}{\rho_0}\frac{\partial\sigma}{\partial S}\left(\frac{\mathrm{d}S}{\mathrm{d}t}\right) = \frac{1}{\rho_0}\frac{\partial\sigma}{\partial\Theta}\left(-\nabla\cdot\boldsymbol{J}^{\Theta}\right) + \frac{1}{\rho_0}\frac{\partial\sigma}{\partial S}\left(-\nabla\cdot\boldsymbol{J}^{S}\right), \tag{3}$$

where $\rho_0$= 1,035 kg m$^{-3}$ is the Boussinesq reference density, $\boldsymbol{J}^{\Theta}$ and $\boldsymbol{J}^{S}$ are subgrid-scale fluxes due to lateral and diapycnal mixing for potential temperature $\Theta$ and salinity $S$, which include surface air-sea buoyancy fluxes and interior diffusion. Substituting the potential temperature and salinity budgets in equation (3) into equation (2) allows us to decompose the diapycnal transformation transports ($\Phi(\sigma)$) into distinct physical processes:

$$\Phi(\sigma) = \Phi\_\mathrm{surf} + \Phi\_\mathrm{vdiff} + \Phi\_\mathrm{ldiff},$$

with each term on the right-hand side representing diapycnal transports due to surface buoyancy fluxes ($\Phi$_surf), interior vertical diffusion ($\Phi$_vdiff), and interior lateral diffusion ($\Phi$_ldiff) of temperature and salinity. Note that there are two conceptually distinct diapycnal diffusive transports appearing in equation (1): Cd($\sigma$) and $\Phi$_vdiff ($\Phi$_ldiff is very small compared to $\Phi$_vdiff in the Equatorial Pacific domain), which are referred to as the "diffusive fluxes" and "diffusive transformation fluxes." These contributions to the net diapycnal transports of $C_{ant}$ are evaluated using diagnostics computed online within the simulation.

In the model, we coarse grain the vertical stratification into four layers guided by the water mass definition of Sloyan et al. (2003): a surface layer ($\sigma < 23$ kg m$^{-3}$), an upper thermocline layer ($23 < \sigma < 24.5$ kg m$^{-3}$), a lower thermocline layer ($24.5 < \sigma < 26.3$ kg m$^{-3}$), and a thermostad layer ($\sigma > 26.3$ kg m$^{-3}$).

## 4. Results: Major Role of Diffusive Transformation Fluxes in Diapycnal Transport of $C_{ant}$

In Figure 1a we show the model meridional-density overturning circulation and its contribution to the $C_{ant}$ budget for the Equatorial Pacific (15°N–15°S) and averaged over a 21 year period (1980–2000) in the surface layer, the upper thermocline, the lower thermocline, and the deeper thermostad layer. The large-scale overturning associated with the STCs transports $C_{ant}$ poleward in the shallow surface layer and equatorward in the thermocline (sum of upper and lower thermocline). Note that there is a relatively strong hemispheric asymmetry in meridional transport across 15°N (S) in the four water mass layers, with this in part being due to the grouping of the Indonesian Throughflow and 15°S transports.

Significantly, we find that $C_{ant}$ in the surface layer over the Equatorial Pacific is largely controlled by the net upwelling transport of $C_{ant}$ across the base of the surface layer ($\sigma$ = 23 kg m$^{-3}$) of 0.4 PgC yr$^{-1}$, which we resolve to be approximately twice the net supply of $C_{ant}$ by air-sea gas exchange (0.203 PgC yr$^{-1}$). This is consistent with the findings of the previous study of Nakano et al. (2015), where reemergence of $C_{ant}$ was identified as a residual, with insufficient diagnostics to attribute the drivers of equatorial upwelling mechanistically.

We examine the processes contributing to the net diapycnal transport of $C_{ant}$ ($\Phi$ + Cd), that is, the contributions from transformation terms due to vertical diffusion ($\Phi$_vdiff), lateral diffusion ($\Phi$_ldiff), surface air-sea buoyancy fluxes (including heat fluxes and freshwater fluxes) ($\Phi$_surf), and the diffusive fluxes (Cd). For a given density, Figure 1b represents the integrated $C_{ant}$ transport across isopycnals, with negative (positive) values indicative of an upwelling (downwelling) due to the diapycnal transport of $C_{ant}$ toward lighter (denser) waters. The net diapycnal transport peaks at the base of the surface layer and then decreases throughout the thermocline (for $\sigma > 23$ kg m$^{-3}$) and has tapered off significantly in the thermostad ($\sigma > 26$ kg m$^{-3}$). Diapycnal transport is dominated by two terms, the vertical diffusive transformation fluxes ($\Phi$_vdiff) and the surface buoyancy fluxes ($\Phi$_surf). Surface buoyancy fluxes transport $C_{ant}$ toward lighter water across all isopycnals ($\Phi$_surf$<$0). The vertical diffusive transformation fluxes ($\Phi$_vdiff) act to counterbalance the upwelling component associated with surface buoyancy fluxes ($\Phi$_surf) in surface waters but reinforce and even dominate the net upwelling of $C_{ant}$ across isopycnals in the thermocline. Compared to these two transformation terms, we find a relatively weak downward diffusive flux of $C_{ant}$ associated with the decrease of $C_{ant}$ concentrations with depth (Cd $>$ 0 across all isopycnals), consistent with the findings of Bopp et al. (2015).

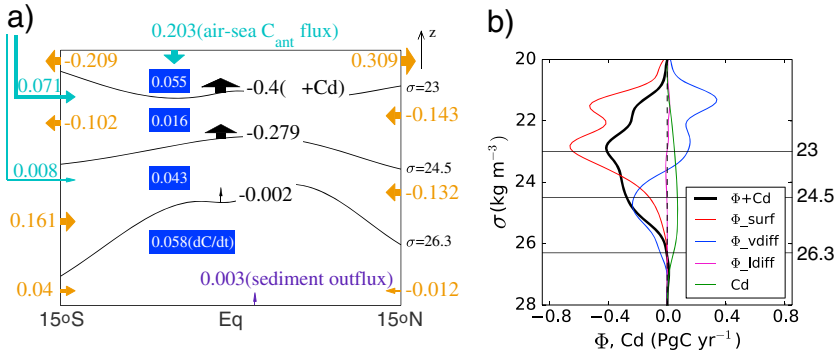


**Figure 1.** (a) Meridional-density overturning circulation for $C_{ant}$ (fluxes in units of PgC $yr^{-1}$) in the Equatorial Pacific. Shown are contributions from net diapycnal transport of $C_{ant}$ (Φ + Cd), black arrows and numbers in the middle, surface air-sea $C_{ant}$ fluxes (cyan arrows and numbers: the L-shaped cyan arrows mean that these two layers outcrop during winter, although isopycnals of $\sigma$ = 23, 24.5 kg $m^{-3}$ are below sea surface on average during the year. These two fluxes of $C_{ant}$ represent exchanges between the outcrops of these layers and the atmosphere.), meridional transports across 15°S(N) (brown arrows and numbers, the transport across 15°S includes the Indonesian Throughflow), sediment outflux from the sea floor (indigo arrow and number), and temporal evolution of $C_{ant}$ inventory in each layer during the period of 1980–2001 (white number with blue background). The values do not add up in each density range due to the temporal evolution of $C_{ant}$ inventory stored in each layer as well as reflecting residual errors associated with the coarse vertical resolution of the model. (b) Net diapycnal transport of $C_{ant}$ (Φ + Cd, in units of PgC $yr^{-1}$) (black thick line), and contributions from transformation terms for vertical diffusion (Φ_vdiff, blue line), lateral diffusion (Φ_ldiff, purple line), and surface buoyancy fluxes (Φ_surf, red line), as well as the diffusive fluxes (Cd, green line). Following the sign convention in the water mass literature, negative (positive) values indicate a transport toward lighter (denser) waters, that is, an upwelling (downwelling).

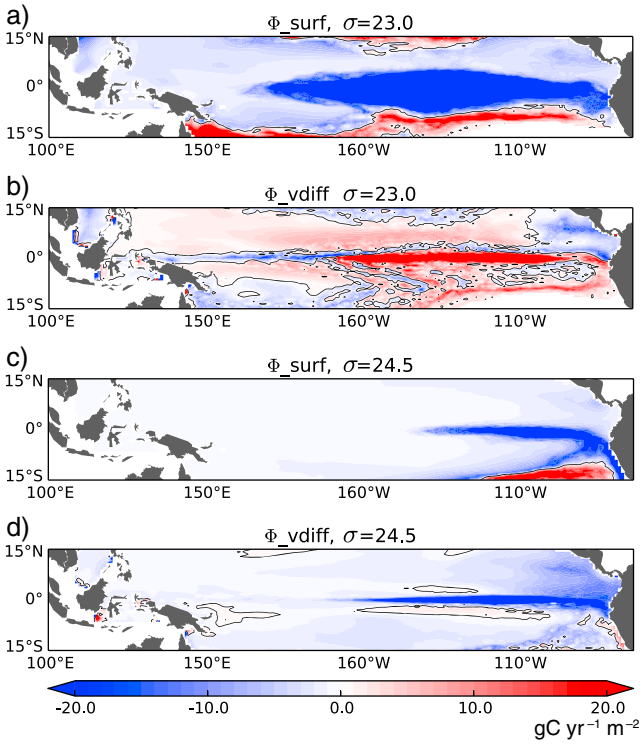


**Figure 2.** Horizontal distribution of diapycnal $C_{ant}$ fluxes due to (a) surface buoyancy fluxes (Φ_surf) and (b) vertical diffusive transformation fluxes (Φ_vdiff) across the base of the surface layer (the isopycnal of $\sigma$ = 23.0 kg $m^{-3}$). (c, d) Same as Figures 2a and 2b but for the midthermocline (the isopycnal of $\sigma$ = 24.5 kg $m^{-3}$) horizon. Each panel has units of gC $yr^{-1}$ $m^{-2}$.

Note that in each layer shown in Figure 1a, the temporal evolution of the $C_{ant}$ inventory should be balanced by the diapycnal transport of $C_{ant}$ across bounded isopycnals, air-sea $C_{ant}$ fluxes, $C_{ant}$ fluxes from seafloor sediments, and the transports across 15°N and 15°S. Nevertheless, residuals (as the $C_{ant}$ budget is not closed) of −0.03, 0.025, 0.019, and 0.005 PgC $yr^{-1}$ in the four layers arise through the transformation diagnostics. As pointed out by Marshall et al. (1999) and Iudicone et al. (2016), such residuals are expected to be a consequence of discretization of equation (2) over the coarse vertical resolution of the numerical model.

Next we consider the spatial patterns of the dominant drivers of diapycnal transport of $C_{ant}$ at the base of the surface layer (across $\sigma$ = 23 kg $m^{-3}$) and in the middle thermocline (across $\sigma$ = 24.5 kg $m^{-3}$) that were identified in Figure 1b. The spatial structure of diapycnal transports of $C_{ant}$ sustained by surface buoyancy fluxes at the base of the surface layer (Figure 2a) reveals a relatively broad upwelling pattern (negative values) and is consistent with the pattern revealed by Bopp et al. (2015). This stands in contrast to the vertical diffusive transformation fluxes at the base of the surface layer (Figure 2b), which exhibit a more equatorially confined downward flux (positive values), thereby opposing the diapycnal transport associated with buoyancy gain. The spatial pattern of diapycnal transport by surface buoyancy fluxes occurs mainly in the central and eastern Equatorial Pacific where the Pacific cold tongue is located. There, large heat fluxes into the ocean have a tendency to transform water toward lighter density classes. The narrow width of the maximum in the vertical diffusive transformation fluxes reflects the width of the Equatorial Undercurrent, where they are sustained by shear instability-induced mixing. When integrated over the full 15°S–15°N domain, the diapycnal transport due to surface buoyancy fluxes is larger than the opposing vertical diffusive transformation fluxes, with this sustaining the net upwelling into the surface layer (Figure 1b).

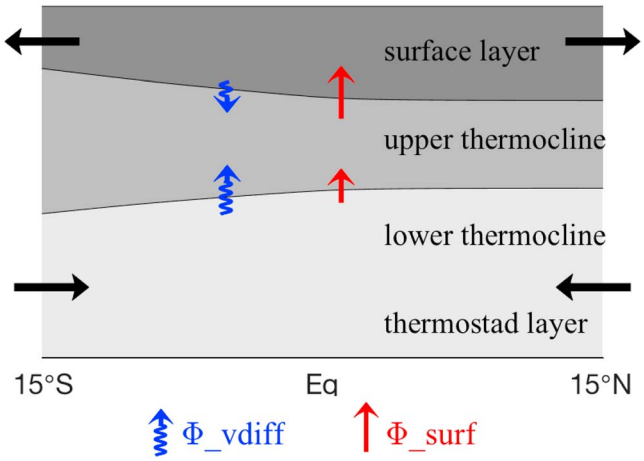


**Figure 3.** Schematic diagram of the two-step process of $C_{ant}$ upwelling from the thermocline to the surface layer. Black arrows represent $C_{ant}$ transports across open boundaries. Upwelling of $C_{ant}$ from lower thermocline to upper thermocline is dominated by Φ_vdiff. Upwelling of $C_{ant}$ from the upper thermocline to the surface layer is dominated by Φ_surf. Note that the vertical blue and red arrows represent integrated values over the Equatorial Pacific. Their position in the figure is not intended to reflect their geographic position.

Within the midthermocline ($\sigma$ = 24.5 kg $m^{-3}$), the upwelling contribution from surface buoyancy fluxes (Figure 2c) is more equatorially confined than the same field at the base of the surface layer (Figure 2a). The diapycnal transport of $C_{ant}$ associated with the vertical diffusive transformation fluxes across the midthermocline (Figure 2d) has in fact changed sign along the equator relative to their role at the base of the surface layer (Figure 2b). The surface buoyancy fluxes and vertical diffusive transformation fluxes are almost equally contributing to reemergence across the midthermocline at the equator, but the role of the surface buoyancy fluxes is diminished in the domain integral due to the positive diapycnal flux (effectively a downwelling in density space) over the region largely south of 10°S and east of 120°W. The diapycnal transport of $C_{ant}$ associated with the vertical diffusive transformation becomes the dominant driver of upwelling across the density horizon over the full domain (Figure 1b). To summarize, upwelling of $C_{ant}$ from waters deeper than midthermocline to the surface layer may be considered to be a two-step process, with the first step dominated by an upward diapycnal diffusive transformation flux across the midthermocline and the second step by the effect of surface buoyancy fluxes across the base of the surface layer. This interpretation is not sensitive to whether the latitudinal extent of the domain for the analysis is 15°S–15°N, as chosen here, or for contracted or expanded latitudinal boundaries (5°S–5°N, 10°S–10°N, 20°S–20°N, Figure S3).

## 5. Discussion and Conclusions

We set out this study to evaluate the mechanistic controls on upwelling/reemergence of $C_{ant}$ over the Equatorial Pacific domain. As a complement to previous studies that have considered $C_{ant}$ re-emergence (Bopp et al., 2015; Iudicone et al., 2016; Nakano et al., 2015), we applied three-dimensional water mass transformation diagnostics to test our hypothesis that diapycnal diffusive transformation fluxes (Φ_vdiff) plays an integral role in the net transport of $C_{ant}$ from the thermocline into surface waters. Our results suggest that the kinematic diagnostics of Bopp et al. (2015) obscured the fundamentally important role of diffusive processes in sustaining upwelling of $C_{ant}$.

In a broad-brush mechanistic view, our results indicate that the upwelling of $C_{ant}$ from thermocline to surface layers of the Equatorial Pacific is best viewed as a two-step process (Figure 3). Between the lower and upper thermocline where Equatorial Undercurrent velocities are the highest (approximately $\sigma$ = 24.5 kg $m^{-3}$), upward transport of $C_{ant}$ toward the surface layers is dominated by vertical diffusive transformation fluxes (Φ_vdiff). By the time $C_{ant}$ approaches the base of the surface layer ($\sigma$ = 23 kg $m^{-3}$), net diapycnal transport of $C_{ant}$ toward even lighter surface waters is dominated by surface buoyancy gain from the atmosphere, through the direct effect of heat and freshwater fluxes (Φ_surf). Thus, it is through the combination of vertical diffusive transformation fluxes and surface buoyancy fluxes that upwelling and reemergence of $C_{ant}$ is sustained.

Our upwelling rate of $C_{ant}$ across the base of the surface layer in the Equatorial Pacific (Φ + Cd = −0.4 PgC $yr^{-1}$, Figure 1) is tightly linked to the time mean volume upwelling rate of 31 Sv in the model, derived with the same water mass transformation framework (Figures S2a and S2b). Previous studies have also estimated a volume upwelling rate in the Equatorial Pacific. Wyrtki (1981) argued that the Ekman divergence and geostrophic convergence in the Equatorial Pacific lead to a volume upwelling rate of 50 Sv. Analysis of bomb-produced radiocarbon indicated that the volume upwelling rate in the Equatorial Pacific region is about 47 Sv (Quay et al., 1983). By using observational data and a box method, Meinen et al. (2001) estimated that the volume upwelling rate in the eastern Equatorial Pacific region is about 24 Sv. Assuming $C_{ant}$ concentrations of 30 mmol $m^{-3}$ and the three previous estimated volume upwelling rates, the corresponding upwelling rates of $C_{ant}$ are 0.57, 0.53, and 0.27 PgC $yr^{-1}$. Therefore, our model estimate of 0.4 PgC $yr^{-1}$ is within a reasonable range compared to these observational estimations.

Given the importance of El Niño variations in the Equatorial Pacific, we are motivated to understand how upwelling of $C_{ant}$ varies with El Niño. The diapycnal transport of $C_{ant}$ at the base of the surface layer shows

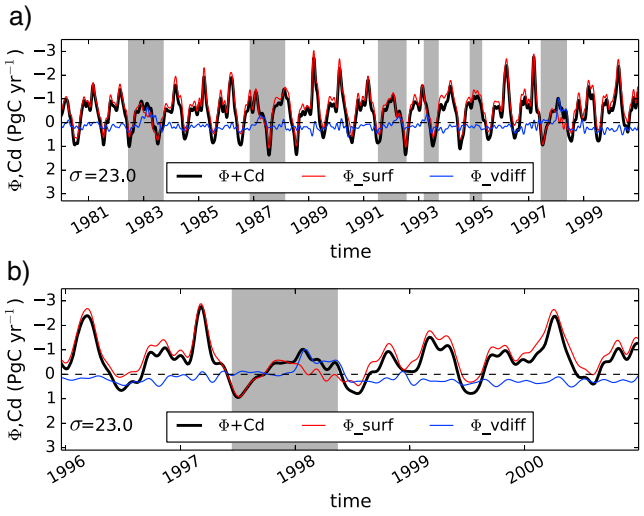


**Figure 4.** Time series of the net diapycnal transport of $C_{ant}$ (thick black line), transformation term associated with the surface buoyancy fluxes (red line) and vertical diffusive transformation fluxes (blue line) at the base of the surface layer over (a) 1980–2000 and (b) 1996–2000. Consistent with the convention in the previous figures, negative fluxes indicate upwelling. The shaded area indicates El Niño events defined when the Niño 3.4 SST index exceeds +0.4°C for a period of 6 months or more (Trenberth, 1997).

strong interannual variability in relation with El Niño (Figure 4). The Niño 3.4 sea surface temperature (SST) index in our simulation and in NOAA observations compare very well with each other (Figure S4a). In addition, the comparison of sea level anomaly between the model and satellite observations indicates that our model captures the interannual variability in the Equatorial Pacific (Figure S4b). We find that the upwelling rate of $C_{ant}$ drops by 50% and 73% during the strong 1982/1983 and 1997/1998 El Niño events, compared with the 21 year (1980–2000) mean value. This response is associated with a strong weakening of the surface buoyancy flux term (Figure 4), due to higher seawater temperature and reduced heat flux into the ocean in the Equatorial Pacific area during El Niño (Figure S5). This reduction of the surface flux-driven upwelling is, however, partly compensated by the diffusive transformation (Φ_vdiff) that switches from a downwelling contribution to an upwelling contribution during El Niño events (Figure 4). The sign switch of vertical diffusive transformation fluxes during El Niño is expected to be caused by deepening of the $\sigma = 23$ kg m$^{-3}$ isopycnal during El Niño.

It is also important to clarify the application of the term "upwelling" in this study in terms of both its spatial and temporal characteristics. For the spatial component, a net diapycnal transport from denser to lighter waters in our analysis does not necessarily reflect an upward vertical motion. For example, westward flowing near-surface water parcels in the South Equatorial Current may be expected to gain buoyancy through surface heat and freshwater forcing. Nevertheless, such water parcels would qualify for upwelling by our definition of cross-isopycnal transports. Likewise, for the temporal component, the apparent seasonal downwelling (positive values) net exchanges of $C_{ant}$ across $\sigma = 23$ kg m$^{-3}$ in Figure 4 do not necessarily correspond to a net downward displacement of water parcels. Rather, it is expected that this diapycnal transport involves displacements of isopycnals, either through a seasonal shoaling of the $\sigma = 23$ kg m$^{-3}$ surface or a lateral contraction of the volume bounded by the $\sigma = 23$ kg m$^{-3}$ surface over the seasonal cycle.

In summary, the $C_{ant}$ upwelling rate from the thermocline to the surface layer is approximately twice as large as the net gain of $C_{ant}$ via air-sea exchange over the Equatorial Pacific domain, underscoring the importance of reemergence of $C_{ant}$ from thermocline waters for the surface layer budget. It is our hope that the identification of density mixing that supplies up-gradient fluxes of $C_{ant}$ from the thermocline to surface waters motivates further investigation that invokes observationally based constraints. Reemergence of $C_{ant}$ in the Equatorial Pacific is of potential importance for its impact on the carbonate buffering capacity of surface seawater, thereby impeding the ocean's ability to further absorb $C_{ant}$ from the atmosphere.

**Acknowledgments**
We thank Samar Khatiwala for the use of observation-based anthropogenic carbon estimates. We thank Carolina O. Dufour for her constructive comments and suggestions on this work. This work was supported by NASA award NNX14AL85G. Partial support for K. B. R. comes through awards NA17RJ2612 and A08OAR4320752, including support through the NOAA Office of Climate Observation, NOAA award NA11OAR4310066. The numerical simulations and analysis were performed with the computational resources of NOAA/GFDL. The MOM5 code described in section 3 is available at https://github.com/mom-ocean/MOM5.

## References

Bopp, L., Lévy, M., Resplandy, L., & Sallée, J. B. (2015). Pathways of anthropogenic carbon subduction in the global ocean. *Geophysical Research Letters*, *42*, 6416–6423. https://doi.org/10.1002/2015GL065073

Dunne, J. P., John, J. G., Adcroft, A. J., Griffies, S. M., Hallberg, R. W., Shevliakova, E., … Zadeh, N. (2012). GFDL's ESM2 global coupled climate-carbon Earth system models, Part I: Physical formulation and baseline simulation characteristics. *Journal of Climate*, *25*, 6646–6665.

Dunne, J. P., John, J. G., Shevliakova, E., Stouffer, R. J., Krasting, J. P., Malyshev, S. L., … Zadeh, N. (2013). GFDL's ESM2 global coupled climate-carbon Earth system models, Part II: Carbon system formulation and baseline simulation characteristics. *Journal of Climate*, *26*, 2247–2267.

Griffies, S. M. (2012), Elements of the Modular Ocean Model (MOM5) (2012 release), GFDL Ocean Group Technical Report No. 7, NOAA/Geophysical Fluid Dynamics Laboratory (pp. 618).

Guilderson, T. P., & Schrag, D. P. (1998). Abrupt shift in subsurface temperatures in the eastern Equatorial Pacific associated with recent changes in El Niño. *Science*, *281*, 240–243.

Halloran, P. R., Booth, B. B. B., Jones, C. D., Lambert, F. H., McNeall, D. J., Totterdell, I. J., & Völker, C. (2015). The mechanisms of North Atlantic $CO_2$ uptake in a large Earth system model ensemble. *Biogeosciences*, *12*, 4497–4508. https://doi.org/10.5194/bg-12-4497-2015

Hauck, J., & Völker, C. (2015). Rising atmospheric $CO_2$ leads to large impact of biology on Southern Ocean $CO_2$ uptake via changes of the Revelle factor. *Geophysical Research Letters*, *42*, 1459–1464. https://doi.org/10.1002/2015GL063070

Iudicone, D., Rodgers, K. B., Stendardo, I., Aumont, O., Madec, G., Bopp, L., … Ribera d'Alcala', M. (2011). Water masses as a unifying framework for understanding the Southern Ocean carbon cycle. *Biogeosciences*, *8*, 1031–1052.

Iudicone, D., Rodgers, K. B., Plancherel, Y., Aumont, O., Ito, T., Key, R., … Ishii, M. (2016). The formation of the ocean's anthropogenic carbon reservoir. *Scientific Reports*, *6*, 35473. https://doi.org/10.1038/srep35473

Key, R. M., Kozyr, A., Sabine, C. L., Lee, K., Wanninkhof, R., Bullister, J. L., … Peng, T.-H. (2004). A global ocean carbon climatology: Results from Global Data Analysis Project (GLODAP). *Global Biogeochemical Cycles*, *18*, GB4031. https://doi.org/10.1029/2004GB002247

Khatiwala, S., Primeau, F., & Hall, T. (2009). Reconstruction of the history of anthropogenic $CO_2$ concentrations in the ocean. *Nature*, *462*(7271), 346–349. https://doi.org/10.1038/nature08526

Large, W. G., & Yeager, S. G. (2009). The global climatology of an interannually varying air-sea flux data set. *Climate Dynamics*. https://doi.org/10.1007/s00382-008-441-3

Large, W. G., McWilliams, J. C., & Doney, S. C. (1994). Ocean vertical mixing: A review and a model with a nonlocal boundary layer parameterization. *Reviews of Geophysics*, *32*(4), 363–403. https://doi.org/10.1029/94RG01872

Le Quéré, C., Rödenbeck, C., Buitenhuis, E. T., Conway, T. J., Langenfelds, R., Gomez, A., … Heimann, M. (2007). Saturation of the Southern Ocean $CO_2$ sink due to recent climate change. *Science*, *316*(5832), 1735–1738. https://doi.org/10.1126/science.1136188

Le Traon, P. Y., Faugere, Y., Hernandez, F., Dorandeu, J., Mertz, F., & Ablain, M. (2003). Can we merge GEOSAT follow-on with TOPEX/Poseidon and ERS-2 for an improved description of the ocean circulation? *Journal of Atmospheric and Oceanic Technology*, *20*(6), 889–895.

Lévy, M., Bopp, L., Karleskind, P., Resplandy, L., Ethe, C., & Pinsard, F. (2013). Physical pathways for carbon transfers between the surface mixed layer and the ocean interior. *Global Biogeochemical Cycles*, *27*, 1001–1012. https://doi.org/10.1002/gbc.20092

Marshall, J., Jamous, D., & Nilsson, J. (1999). Reconciling thermodynamic and dynamic methods of computation of water-mass transformation rates. *Deep-Sea Research Part I*, *46*, 545–572.

Meinen, C. S., McPhaden, M. J., & Johnson, G. C. (2001). Vertical velocities and transport in the Equatorial Pacific during 1993–99. *Journal of Physical Oceanography*, *31*, 3230–3248.

Nakano, H., Ishii, M., Rodgers, K. B., Tsujino, H., & Yamanaka, G. (2015). Anthropogenic $CO_2$ uptake, transport, storage, and dynamical controls in the ocean imposed by the meridional overturning circulation: A modeling study. *Global Biogeochemical Cycles*, *29*, 1706–1724. https://doi.org/10.1002/2015GB005128

Pascual, A., Faugere, Y., Larnicol, G., & Le Traon, P. Y. (2006). Improved description of the ocean mesoscale variability by combining four satellite altimeters. *Geophysical Research Letters*, *33*, L02611. https://doi.org/10.1029/2005GL024633

Quay, P. D., Stuiver, M., & Broecker, W. S. (1983). Upwelling rates for the Equatorial Pacific Ocean derived from the bomb $^{14}C$ distribution. *Journal of Marine Research*, *41*, 769–792.

Rodgers, K. B., Aumont, O., Madec, G., Menkes, C., Blanke, B., Monfray, P., … Schrag, D. P. (2004). Radiocarbon as a thermocline proxy for the eastern Equatorial Pacific. *Geophysical Research Letters*, *31*, L14314. https://doi.org/10.1029/2004GL019764

Sabine, C. L., Feely, R. A., Gruber, N., Key, R. M., Lee, K., Bullister, J. L., … Rios, A. F. (2004). The oceanic sink for anthropogenic $CO_2$. *Science*, *305*, 367–371.

Sarmiento, J. L., Hughes, T. M. C., Stouffer, R. J., & Manabe, S. (1998). Simulated response of the ocean carbon cycle to anthropogenic climate warming. *Nature*, *393*, 245–249.

Schwinger, J., Tjiputra, J. F., Heinze, C., Bopp, L., Christian, J. R., Gehlen, M., … Totterdell, I. (2014). Nonlinearity of ocean carbon cycle feedbacks in CMIP5 Earth system models. *Journal of Climate*, *27*(11), 3869–3888.

Sloyan, B., Johnson, G., & Kessler, W. (2003). The Pacific cold tongue: A pathway for interhemispheric exchange. *Journal of Physical Oceanography*, *33*, 1027–1043.

Trenberth, K. E. (1997). The definition of El Niño. *Bulletin of the American Meteorological Society*, *78*, 2771–2777.

Wyrtki, K. (1981). An estimate of equatorial upwelling in the Pacific. *Journal of Physical Oceanography*, *11*(9), 1205–1214.